RSC Mechanochemistry

ROYAL SOCIETY OF CHEMISTRY

PAPER

View Article Online
View Journal | View Issue

Cite this: *RSC Mechanochem.*, 2025, **2**, 723

Chemical models to map the transformation from precursors to semiconductor materials at non-equilibrium conditions†

Hugo Rojas-Chávez *

Received 6th May 2025
Accepted 13th June 2025

DOI: 10.1039/d5mr00061k

rsc.li/RSCMechanochem

This work proposes the construction of chemical models based on the Gibbs composition triangle, which provides support for the proper interpretation of semiconductor synthesis under non-equilibrium processing, considering the pertinent variables of the system. It demonstrates how chemical models are constructed using experimental findings and theoretical insights and by incorporating data available in the literature. Then, an illustrative example is used to validate the construction, interpretation and application of a chemical model for obtaining PbTe *via* non-equilibrium process. This approach can be directly applied to forecast the formation of IV–VI and II–VI binary semiconductors, as well as the formation of ternary semiconductor solid solutions. However, it is exemplified—in this work—*via* the mechanochemical synthesis of PbTe. This work aims to construct a chemical model that maps the transformation from precursors to semiconductor material through the high-energy milling process.

Introduction

Over the last decade, the research, development, and production of materials and alloys have intensified, significantly improving our daily lives. Most of the alloys obtained are based on phase diagrams because they can assist in designing experimental routes to obtain certain phases with intriguing properties. Phase diagrams also allow for determining the behavior—thermodynamic stability—of the different phases involved in a system. In other words, they can help us understand how temperature, pressure, and composition affect the microstructure in specific phases. For this reason, phase diagrams are indispensable for the development of alloys, which are widely applied in various fields of science and technology.

The phase diagrams are considered roadmaps that denote the relationships between the phases present, temperature, pressure, and composition that occur under specific processing conditions. If the phase diagram of an alloy system is known, then the preparation of the alloy with desired properties can be controlled. In practice, the use of phase diagrams avoids the experimental trial-and-error method, which costs considerable time, effort, and resources. Additionally, phase diagrams have applications in manufacturing, such as thermomechanical processes and heat treatments, among others.

Although phase diagrams are currently used to obtain alloys at or near equilibrium conditions,[1,2] significant advancements have been made in the field of phase diagrams nowadays. For instance, theoretical modelling of phase diagrams of nanomaterials,[3,4] nanoalloy phase diagrams,[5] size-dependent phase diagrams,[6,7] among others, provides new opportunities not only in understanding new systems but also in materials design.[4,8,9] Unambiguously, the results obtained using computer simulations and/or experimental findings are necessary for calculating and constructing more reliable phase diagrams of alloy systems.[10–13]

Until now, most experimental routes to obtain materials and systems at equilibrium have focused on phase diagrams, but alternatives to non-equilibrium processing conditions are lacking. It is essential to note that, over the last few decades, non-equilibrium processes have taken advantage of the versatility of precursor and reaction parameters (such as processing time, room temperature, atmospheric conditions, and multi-step strategies) to produce unique nanomaterials for the fabrication of increasingly impressive nanodevices.[14–17] Unfortunately, there is insufficient literature available for the interpretation and application of graphical methods, such as phase diagrams, in materials production *via* non-equilibrium processes. It is well known that reported phase diagrams, thermodynamic databases, and specialized scientific software are frequently used to design experimental routes for obtaining alloys with specific phases. Lamentably, that kind of data, including graphical methods (road maps), in systems not at equilibrium are scarce. For that reason, to construct diagrams for alloy production *via* non-equilibrium processes remains a challenge in materials science and related fields.

Tecnológico Nacional de México, Instituto Tecnológico de Tláhuac II, Camino Real 625, Col. Jardines del Llano, Alcaldía Tláhuac 13550, San Juan Ixtayopan, Mexico. E-mail: hugo.rc@tlahuac2.tecnm.mx

† Electronic supplementary information (ESI) available. See DOI: https://doi.org/10.1039/d5mr00061k

This work aims to construct chemical models (roadmaps) that map the transformation from precursors to semiconductor materials through the high-energy milling (HEM) process, which is currently achieved *via* synthesis under non-equilibrium conditions. Such chemical models are usable and compatible, in terms of comprehension, with current processing practices. Additionally, this proposal opens up new opportunities for visualizing the chemical pathway during the synthesis of semiconductors under non-equilibrium conditions.

Preliminary considerations

When non-equilibrium conditions are considered during the processing of materials, the data reported in phase diagrams may be inconsistent with experimental findings, *i.e.*, phase and microstructure changes are not reasonably explained. Therefore, phase diagrams cannot assist in forecasting phase relations, compositional changes and structures in systems under far-from-equilibrium conditions. Thus, non-equilibrium processing of materials often differs significantly from the data available in phase diagrams. However, the transformation from precursors to semiconductor materials can be traced by considering three significant reaction stages during the mechanochemical synthesis of IV–VI and II–VI binary semiconductors, including the formation of ternary semiconductor solid solutions; namely, (1) oxidation, including reoxidation of precursors, (2) chemical interaction between both metal and chalcogen suboxides to give way to stoichiometric complex oxides and (3) chemical reduction of that complex oxides to obtain semiconductor materials. Such a series of both solid–solid and gas–solid reactions are generated in the course of the HEM process, and the reaction products are obtained at specific prefixed milling time by considering local equilibria.[18]

Experimental considerations

As is known, during milling, sampling is performed by taking powder-milled mixtures from the vial at several prefixed periods of processing time to characterize the as-milled sample to permit researchers gaining an in-depth understanding of the relationship between milling time and coexisting phases at all length scales, including bulk and surface one, see ESI† for further details on sample preparation. For phase non-equilibrium studies, standard bulk experimental techniques are required, *e.g.*, X-ray diffraction (XRD), secondary ion mass spectrometry (SIMS), electron-probe microanalysis (EPMA), and scanning electron microscopy (SEM), among others. Additionally, the former must be supplemented with accurate surface experimental measurements, *e.g.*, high-resolution transmission electron microscopy (HRTEM), scanning transmission electron microscopy (STEM), and X-ray photoelectron spectroscopy (XPS).

As reported in the literature, the experimental findings obtained through bulk and surface measurements have, in fact, begun to serve as a guide at each prefixed processing time.[18–22] Under composition, pressure, and temperature (c–P–T) vial conditions, it enables an analysis of the significant relationship between interatomic chemical interactions and phase transitions that occur in materials with varying milling times. Then, when the structure and composition of all phases in a system are known as a function of processing time, considering local equilibrium, a preliminary chemical model can be proposed to forecast the formation of a material. A detailed description of the relevant data of each phase in this case study can be found in the ESI.†

Theoretical considerations

Emphasis is placed on describing aspects that involve chemical transformations during the HEM process through the graphical representation approach, *i.e.*, the chemical model. To demonstrate how local and overall chemical kinetics contribute to the global transformations from precursors to the final product, a framework of experimental and theoretical reactions is proposed as a function of milling time in accordance with the thermodynamic data available in the literature.[19,23,24] Lastly, a thorough explanation of the phase transition chemical pathway linked to the non-equilibrium process, from precursors to product, can be proposed. Consequently, the chemical model involves an interpretation whose forecasts are verified through experimental findings, theoretical data, and even analogous and ideal phases that have not been documented to date. It is worth mentioning that possible gas phases were considered in terms of Gibbs free energy.[19,23,24]

Chemical model construction

Based on experimental findings and theoretical considerations, it is established that the chemical model encompasses three primary stages associated with a series of phases, which are a function of both milling atmosphere (oxygen potential) and processing time, provided that precursors are poured under atmospheric conditions.[18–22] In addition to this, the formation of semiconductors *via* a non-equilibrium process results from an interplay between physico-metallurgical and mechano-chemical stimuli.[23] The first kind of stimulus tends to favor agglomeration of particles because of the Van der Walls forces, dis-agglomeration and re-agglomeration of tiny particles, plastic deformation, fracture and mechanical kneading as well. The second kind is related to the oxidation and reoxidation of precursors, intermediate reactions, and transitions where crystalline, amorphous, and/or non-stoichiometric phases are formed at different scales. The interaction between physico-metallurgical and mechano-chemical stimuli has resulted in the production of semiconductors with increasingly more elaborated shapes and structures when specific process control agents (PCA) are used.[25–28]

A chemical model is constructed using slice cuts, which are a function of processing time, considering oxygen potential while taking into account other parameters (*e.g.*, type of mill, milling media, vial composition, PCA addition, *etc.*). Such slice cuts of the chemical model reveal the phases present associated with a specific processing time, which, in turn, allows us to infer

the chemical reactions undergone by the precursors (Fig. 1). Therefore, to avoid the presence of impurities during the semiconductors processing, an inert experimental setup is taken into consideration, see the ESI† for further details on sample preparation.[18–25,27,28]

Example of construction and discussion

The proposal of graphical methods to describe materials formation adequately at non-equilibrium processing conditions is lacking, hindering the design of experimental routes to obtain specific materials with desired properties. Currently, there is no proposal to address this topic, making it difficult for researchers to visualize a possible path related to non-equilibrium processes. Therefore, to establish how, during milling, a system is driven from precursors to a mixture of phases, including oxides, hence to the desired semiconductor, a chemical model is constructed.

General features for the construction of the chemical model

In this work, it is shown that an appropriate chemical model for the mechanochemical synthesis of PbTe can be constructed using both bulk and surface characterization, supplemented with theoretical data reported in the literature. This approach considers milling time and thermodynamic data available in the literature, as shown in Fig. 2.

At this point, starting from the very basics, it is important to keep in mind that although the Pb–Te system is the main, oxygen must be taken into account due to the milling is carried out under an air atmosphere and/or because it is present in the precursors (*e.g.*, lead oxide). As a consequence, the Pb–Te–O system is considered the central system in the Gibbs composition triangle, as shown in Fig. 2a. As shown in this figure, it can be inferred that apexes represent pure substances, *i.e.*, Pb, Te, and O. Moreover, three binary systems are given in the Gibbs composition triangle as Pb–O, Pb–Te and Te–O. Then, after

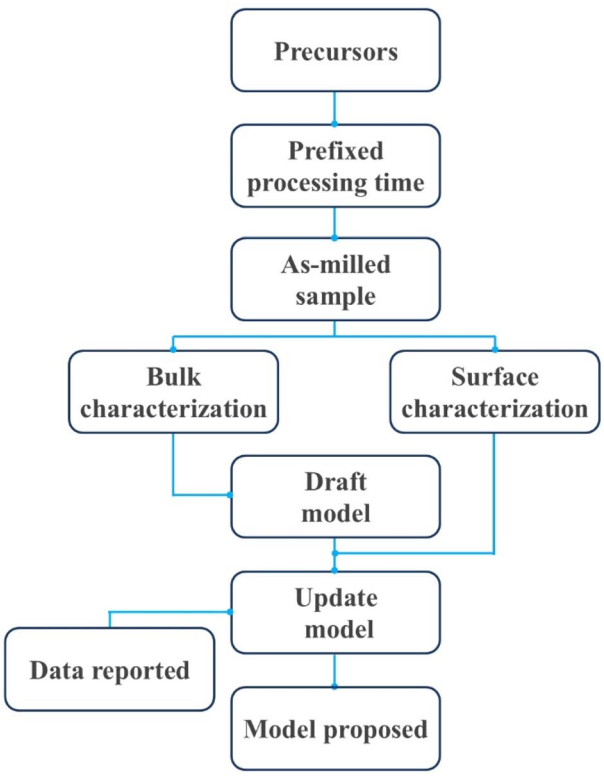

Fig. 1 Schematic summarizing the chemical model construction used to obtain a description for the mechanochemical synthesis of semiconductors.

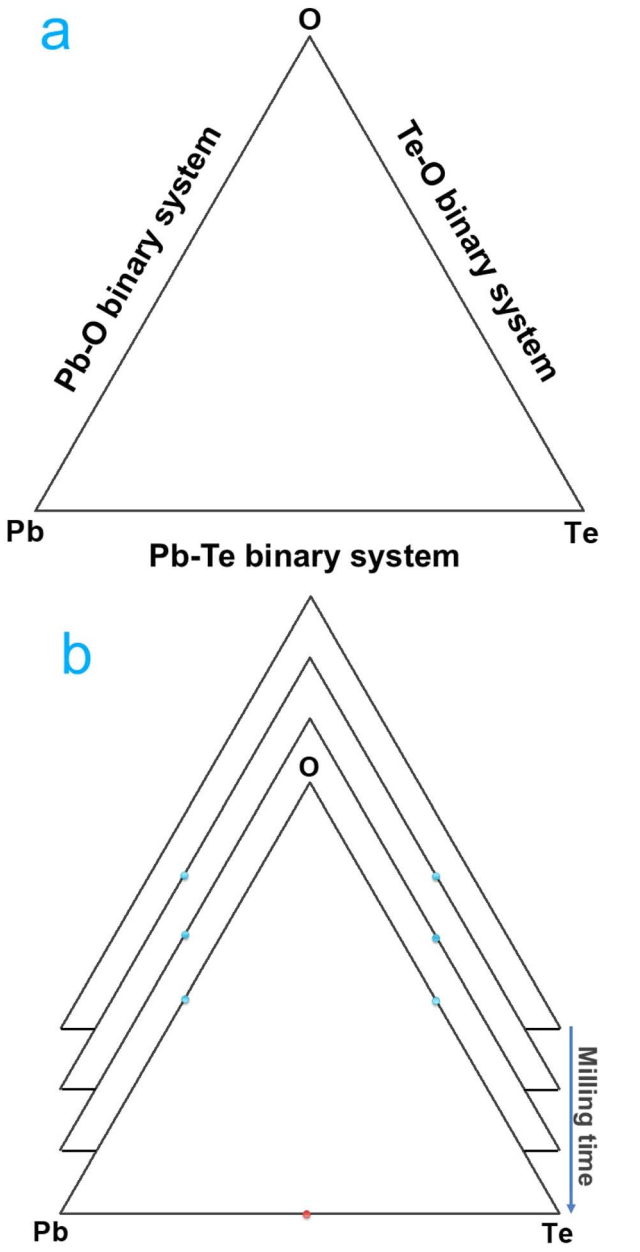

Fig. 2 (a) Schematic initial chemical model construction. (b) Schematic overlay of the experimental findings traced as a function of the processing time.

each prefixed milling time, the experimental stoichiometric phases detected can be consecutively located in the Pb–Te–O system and/or along their respective binaries (see Fig. 2b). A detailed description of the relevant data for each phase can be found in the ESI.†

Location of phases in the chemical model

The first stage, the initial chemical condition, is denoted by the starting point S_i, which depends on the chemical composition of the precursors. For instance, if PbO and Te are the precursors, S_i will be denoted by I. On the contrary, if Pb and Te are the precursors, S_i will be denoted by II, as shown in Fig. 3a.

As shown in Fig. 3b, due to milling being carried out under an air atmosphere, oxidation or reoxidation of the precursors is expected. Consequently, phases are arranged in the Pb–Te–O system according to the usual chemical formulae of the substances. Furthermore, as can be noted in the Pb–O and Te–O binary systems, Pb- and Te-oxides are located as molecular stoichiometric species, which depend on the oxygen content. It is worth noting that extreme Te-oxidation did not occur during the HEM process.

As the milling time progresses, Pb- and Te-oxides react with each other to form a complex oxide with the maximum quantity of oxygen. In this case, it is represented by $PbTeO_3$, which is stoichiometrically balanced (see Fig. 4a). As can be noted,

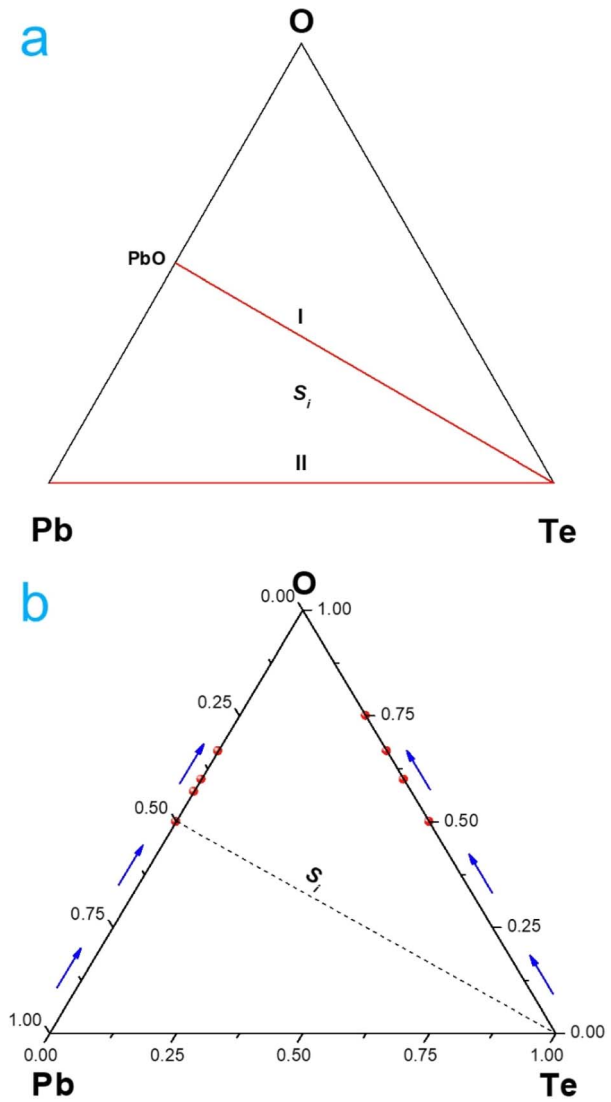

Fig. 3 (a) Schematic representation of the initial chemical condition S_i. (b) Oxidation condition with respect to precursor compositions. Note that arrows represent the increment of the oxygen potential.

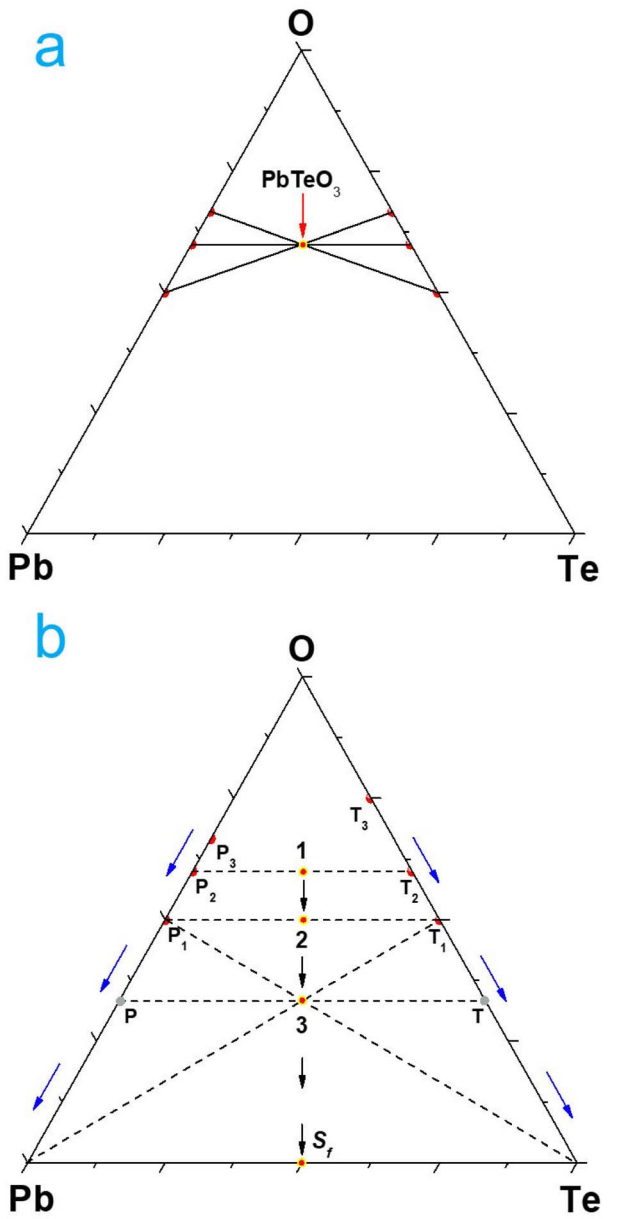

Fig. 4 (a) Nodal convergence of equivalent oxygen potential conditions represented by $PbTeO_3$. (b) Hypothetical reduction reaction path from 1 to S_f to transform $PbTeO_3$ into PbTe. Note that S_f is the ending point, and arrows represent the decrement of the oxygen potential. Furthermore, note that the points P, P_1, P_2 and P_3 correspond to the Pb_2O, PbO, Pb_3O_4, Pb_2O_3 and PbO_2 oxides, while the points T, T_1, T_2 and T_3 are associated with the Te_2O, TeO, TeO_2 and TeO_3 ones.

$PbTeO_3$ can be obtained in several ways. Hence, it is considered a nodal chemical condition due to several interactions among lead and telluride stoichiometric oxides that can occur. It is worth highlighting that the use of the Gibbs composition triangle for this proposal requires that each of the identified phases is defined by a sum of 1, which can be readily verified.

Once the maximum oxygen condition is reached, then the reduction condition takes place (see Fig. 4b). The 1–3 points, aligned along the O–PbTe direction, are associated with chemical compositions satisfying the following stoichiometric ratios: $PbTeO_3$, '$PbTeO_2$' and 'PbTeO', respectively. In general, it can be understood that along the O–PbTe direction, a decomposition reaction takes place, as has been reported in the literature.[29] As shown in Fig. 4b, it can be further appreciated that along the Pb–O binary system, points P, P_1, P_2 and P_3 correspond to the Pb_2O, PbO, Pb_3O_4, Pb_2O_3 and PbO_2 oxides, respectively. In this sense, the points T, T_1, T_2 and T_3 are associated with the Te_2O, TeO, TeO_2 and TeO_3 oxides, respectively. It is worth noting that the phases related to P and T – in the Gibbs composition triangle – have not been experimentally detected, but they serve as reference points.[19,20] However, the phase related to T_3 was superficially detected (see the ESI†).

Depuration of the chemical model

The Pb–O system has been assessed by different authors,[30–33] it is interesting to note that during the thermal decomposition of PbO_2, several oxides, per lead atom have been reported in the PbO–PbO_2 range (*i.e.*, $PbO_2 \rightarrow PbO_{1.89} \rightarrow PbO_{1.59} \rightarrow PbO_{1.43} \rightarrow PbO_{1.29} \rightarrow PbO$).[31] As can be noted, there is a deviation from the ideal stoichiometry of the Pb-oxides. For instance, the Pb_3O_4 is in the $PbO_{1.43}$–$PbO_{1.29}$ range, while the Pb_2O_3 is in the $PbO_{1.59}$–$PbO_{1.43}$ range.[31] Consequently, the P point should be considered as a reference point, as it has not been reported in the literature,[30–33] see Fig. 4b.

Regarding the Te–O system, oxides richer in oxygen have been reported in the literature.[34–36] However, neither TeO_3 nor TeO_4 has been detected in bulk quantities during the HEM process. In this context, point T should be considered as a reference point because it has not been reported in the literature,[19,20] see Fig. 4b. In addition to this, due to extreme Te-oxidation did not take place during the mechanochemical synthesis of PbTe,[19,20] then the point T_3 should also be considered as a reference point, which was superficially detected, see the ESI.† For the Te–O system, the oxygen content in the tellurium oxides, per tellurium atom, in the TeO–TeO_3 range follows the trend $TeO_3 \rightarrow TeO_2 \rightarrow TeO$. It is worth noting that the Pb–Te system has also been reviewed.[36,37]

As shown in Fig. 3 and 4, once a primary arrangement of the phases is roughly proposed, where all substances are in their corresponding placements, the depuration of the chemical model must be addressed, considering both experimental findings (as a function of milling time) – and thermodynamic data reported in the literature. For instance, in the Gibbs composition triangle, initially, only the solid stoichiometric phases detected are located in the Pb–Te–O system, see Fig. 3 and 4. For that reason, along the Pb–O binary system, PbO and PbO_2 are considered, while alongside the Te–O binary system, TeO and TeO_2 are regarded. In the case of the Pb–Te binary system, PbTe is included. Finally, in the Pb–Te–O ternary system, $PbTeO_3$ is considered, see Fig. 4.

Interpretation of the chemical model

As shown in Fig. 5, the interpretation of the chemical model, with brief explanations, is straightforward. For instance, inside the Gibbs composition triangle, the 1–3 points, aligned along the O–PbTe direction, are associated with chemical compositions satisfying the following stoichiometric ratios: $PbTeO_3$, '$PbTeO_2$' and 'PbTeO'. It is interesting to remark that the a′ point ('$PbTeO_4$') is also aligned along the O–PbTe direction. In general, it can be understood that along the O–PbTe direction, a decomposition reaction takes place, as has been reported in the literature.[29] Therefore, the 1–3 points up to the S_f point denote the synthesis path to obtain PbTe through a non-equilibrium process since S_i denotes the starting point. It can be further appreciated that quoted phases have not been detected experimentally during the mechanochemical synthesis of PbTe.[19,20]

Investigating in literature the quoted phases closely, it should be noted that although the $PbTeO_3$ is the most stable product of the oxidation during milling, data reported in the literature indicate that '$PbTeO_4$' could be favored under the influence of specific parameters of temperature and oxygen partial pressure,[38,39] such phase could be associated with the TeO_3 presence.

To simplify the synthesis path related to the non-equilibrium processes, by situating only those phases identified *via* experimental findings,[19,20] it can be clearly seen that there is an internal triangle—into the Gibbs composition triangle—which describes the PbO–$PbTeO_3$–PbTe relationship, see Fig. 5. Thus,

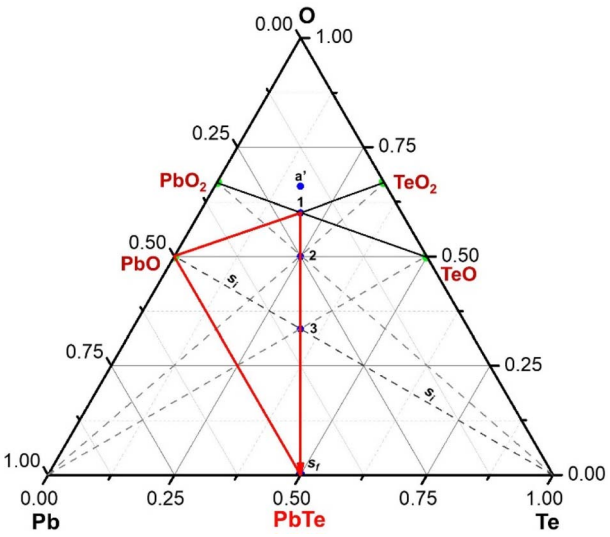

Fig. 5 Schematic chemical model depiction of the Pb–Te–O system for the mechanochemical synthesis of PbTe, considering solid phases. Note that (i) point 1 represents $PbTeO_3$ stoichiometrically balanced, (ii) S_i is the starting point, and (iii) S_f is the ending point.

the proper interpretation of results obtained can be described as follows: in the light of experimental findings, it can be inferred that $PbTeO_3$ is the result of the 'addition' of PbO plus TeO_2. In this context, TeO_2 can only be obtained if PbO is reduced by Te. Additionally, to understand formation of TeO_2 the formation, gaseous species must be considered in accordance with the thermodynamic data available in the literature.[19,23,24] As shown in Fig. 6, TeO (g) or Te_2O_2 (g) must be regarded as an intermediate state between TeO (g)/Te_2O_2 (g) to TeO_2. It is worth emphasizing that (i) these transitions are situated on the Te–O binary, (ii) the most important reactions are those where point 1 is situated and (iii) reaction among TeO_2–TeO (Te_2O_2)–Te should be considered in conformity with the thermodynamic data available in the literature.[19,23,24] Through inherent calculations, a triple point provided by the phases PbO, $PbTeO_3$ and PbTe will be in equilibrium at a particular temperature.[19,20] It is worth mentioning that equilibria change as a function of processing temperature is due to the following gaseous species: either TeO_2 (g) or TeO (g)/Te_2O_2 (g) *versus* (Te), in conformity with the thermodynamic data available in the literature.[19,23,24]

A straightforward way to discern this is that theoretical insights and experimental results allow us to propose that the TeO_2 (gas or solid), TeO (g)/Te_2O_2 (g), and Te_2 (g) are a series of reduction steps encompassed in the progressive reduction of lead oxides.[19,23,24] To the extent that higher oxygen potentials predominate in the vial in comparison to those to trace TeO (g)/Te_2O_2 (g), $PbTeO_3$ will be associated with PbO, while lower oxygen potentials will undergo a transition where in place of interaction between PbO–TeO_2 a sequence will take place as follows: Pb–TeO (g)/Te_2O_2 (g) and Pb–TeO–(Te_2). As shown in Fig. 6, the partial pressure of Te_2 (g) will be in charge of reducing any Te- and/or Pb-oxides that are still present after the oxygen potential has been reduced to the smallest possible level, which will result in the formation of PbTe.[19,23,24]

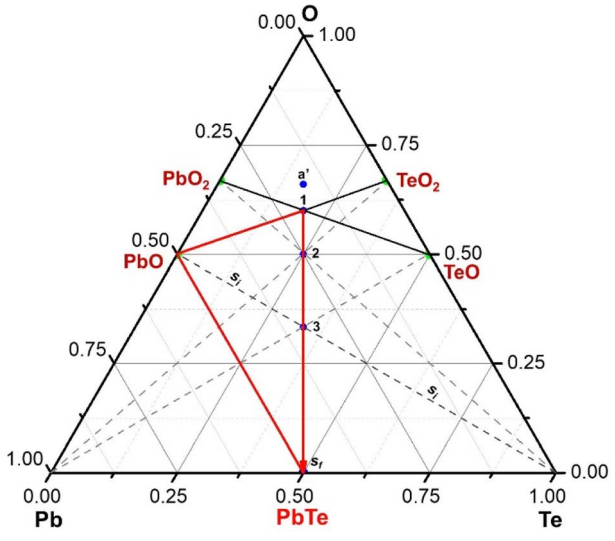

Fig. 6 Schematic chemical model depiction of the Pb–Te–O system for the mechanochemical synthesis of PbTe, considering both solid and gaseous phases. Note that (i) point 1 represents $PbTeO_3$ stoichiometrically balanced, (ii) S_i is the starting point, and (iii) S_f is the ending point.

The kinetics of converting raw materials into PbTe show that the formation of PbTe is highly favored even at the early stages of the non-equilibrium process, which is of practical significance considering that the thermodynamic and chemical mechanisms previously discussed are self-consistent with theoretical data and experimental findings.[19,24] However, based on thermodynamics, the presence of oxygen-containing phases predominates up until the point where oxides give way to the complete transformation of PbTe, taking into consideration the occurrence of the triple phase unalterable point, PbO–$PbTeO_3$–PbTe. It is essentially important to note how the Pb–Te–O system's phases are grouped; this triangular representation illustrates a high degree of symmetry between oxides and PbTe. Consequently, information on this model illustrates how two types of heterogeneous oxides are associated with the PbTe.

A comment worth mentioning is that physical-metallurgical stimuli, such as plastic deformation and structural defects, should be considered as stored energy during the non-equilibrium process. Chemical crystal transitions, which may be primarily considered as entropic changes in the system, could be encouraged by such stimuli. In terms of mechanochemical stimuli, deformed PbO in close contact with Te causes a reduction of the former phase in restricted locations, including the nano- and microscale, due to the distinct mechanical reactions of the reactant particles. A transition balance between PbO, Te, TeO (or Te_2O_2), and TeO_2 (gas or solid) would be established attributable to the negative free energy of formation of the Te-enriched phases,[19,20,24] revealing $PbTeO_3$ as an intermediate as-milled reaction product. Nevertheless, the gaseous tellurium overrides the partial pressure of oxygen during the milling process, giving rise to PbTe.[19,20,23,40]

The O–PbTe path allows for a schematic representation of how, in theory, it may progress from the 1 point to the S_f one once the highest oxygen chemical potential is achieved. Thus, the stages through these transitions are defined as follows: $PbTeO_3$ → $PbTeO_2$ → PbTeO → PbTe, as proposed in the literature.[20,29]

The PbO–Te pseudo-binary system

To supplement the schematic chemical model representation of the Pb–Te–O system for obtaining PbTe, a graphic depiction of the pseudo-binary PbO–TeO_2 local equilibrium is proposed to enrich the understanding of the mechanochemical synthesis of PbTe, see Fig. 7. In this graphic representation A_1, C_1 and F_1 have been unambiguously detected by the XRD technique.[19,20,24] Additionally, with the same technique supplemented by SIMS,[41] C_5 has been extensively identified, and this result has also been confirmed by the EDS elemental map technique.[28] In what surface characterization is concerned, C_1, C_4, C_5 and F_1 have been detected by EDX-STEM, SAED and XPS techniques.[19,28,41] It is worth highlighting that B_1, D_1, and E_1 have not been detected by any experimental technique during milling, but B_1 and E_1 have been reported in the literature.[42,43]

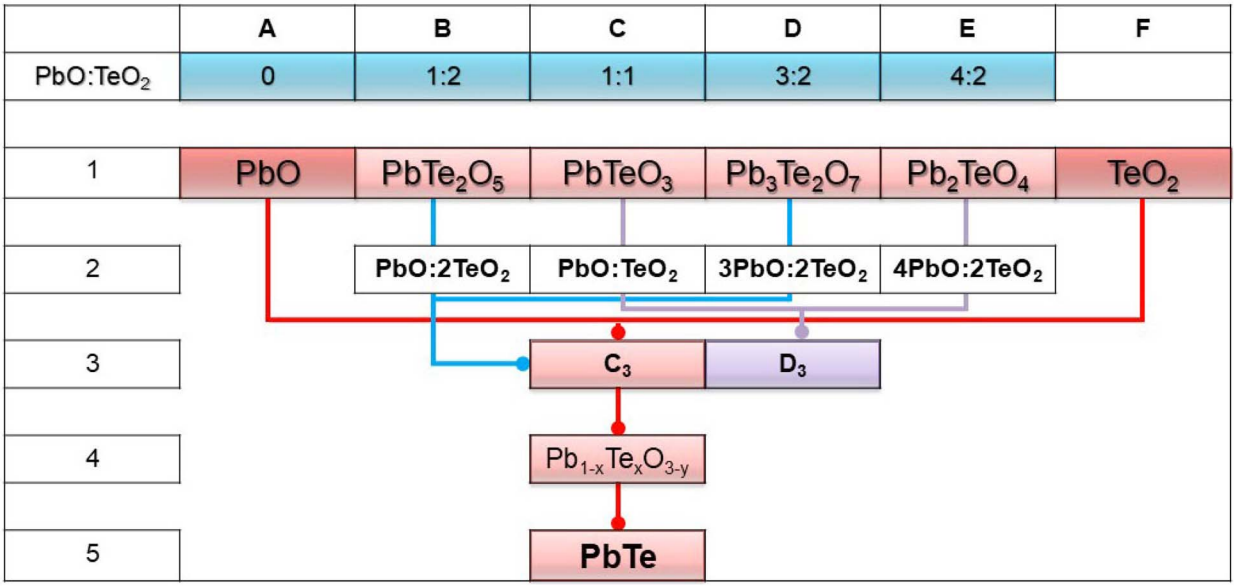

Fig. 7 Schematic depiction illustrating the chemical interactions in the pseudo-binary PbO–TeO_2. Note that the as-milled products are placed as stoichiometric, non-stoichiometric, experimental, and theoretical or even undetected complex oxides. The PbO : TeO_2 row indicates the molar ratio of the intermediate reaction products.

As shown in Fig. 7, it illustrates that the pseudo-binary PbO–TeO_2 local equilibrium makes it evident how the addition of its contiguous phases yields intermediate oxides. As a result, it is feasible to recognize a set of pair interactions between A and F, which enable the formation of intermediate oxides, specifically C_3 and D_3. Note that the 1 point—in Fig. 6—is represented as C_3 in Fig. 7. It is worth mentioning that C_3 can be obtained in two diverse ways. In the first case, by the addition of its adjacent phases (B_1 and D_1) and second, by adding the extremes (A_1 and F_1). Another intriguing feature is that D_1 is not governed by the addition of its adjacent phases, as previously established.

Fig. 7 schematically illustrates the decrease in oxygen chemical potential in the oxides between A_1 and F_1 (row one → row three → row four → row five). In this regard, a more thorough analysis revealed that rows 1 and 2 correspond to equivalent phases in Fig. 7. Row 3 suggests that when the PbO : TeO_2 ratio is equal to 1.0, $PbTeO_3$ can be formed. Furthermore, the same result can be achieved when the undetected phases (B_1 and D_1), which represent the maximum oxygen chemical potential, are added. It is key to point out that, in this latter case, the PbO : TeO_2 ratio is also equal to 1.0.

Finally, it is expected that the oxygen potential decreases as follows: $PbTeO_3$ → $Pb_{1-x}Te_xO_{3-y}$ → PbTe (C_1 → C_4 → C_5), noting that this trend—in Fig. 7—is located along the O–PbTe direction in Fig. 6. It is worth noting that the high-energy collisions, during milling, give way to c–P–T vial conditions, which change the rate and outcome of the phase transformations, as the milling time proceeds, and may result in the appearance of unusual states or phases, distinct to those expected under typical equilibrium processing conditions.[29] The $Pb_{1-x}Te_xO_{3-y}$ is an example of those unusual phases; it is an amorphous or non-stoichiometric phase which is formed under the following condition: pO_2 ($PbTeO_3$) > pTe_2.[19,23]

In simple terms, due to chalcogen possessing close chemical similarities, because the elements in the same group of the periodic table have similar chemical properties, they have been treated as "rock-salt IV–VI semiconductors" since their characteristics do not differ from each other. Therefore, as shown in the ESI,† considering equivalent systems (*e.g.*, Pb–Se–O) as well as processing parameters, reasonable analogous chemical models can be generated, including the formation of ternary semiconductor solid solutions and II–VI semiconductors (*e.g.*, ZnTe).

Conclusions and outlook

A chemical model has been constructed to map the transformation from precursors to PbTe semiconductor material at non-equilibrium processing conditions under an air atmosphere, taking milling time into consideration. The interpretation of the chemical model allows us to visualize the chemical pathway from precursors to the semiconductor without the need for specialized software, facilitating understanding, in detail, about the obtaining of PbTe semiconductors through non-equilibrium process conditions.

The chemical model permits a closer look at the chemical interactions among the phases, facilitating phase correlation during milling. In fact, to supplement the schematic chemical model representation of the Pb–Te–O system for the mechanochemical synthesis of PbTe, a graphic representation of the pseudo-binary PbO–TeO_2 local equilibrium was proposed to provide a more complete picture.

An important outcome is that the chemical model, based on the Gibbs composition triangle, provides enough experimental and theoretical data to understand the synthesis path related to the non-equilibrium process. Furthermore, the usage of such

chemical models is not limited to the proposed system. Additionally, considering equivalent systems (*e.g.*, Pb–Se–O) as well as processing parameters, reasonable analogous chemical models can be generated, including the formation of ternary semiconductor solid solutions. Therefore, this proposal presents new opportunities for visualizing the chemical pathway during the synthesis of semiconductors under non-equilibrium conditions.

Data availability

Data will be made available on request.

Author contributions

Conceptualization, investigation, formal analysis, visualization, writing – original draft, writing review and editing: H. Rojas Chávez.

Conflicts of interest

There are no conflicts to declare.

Acknowledgements

The author appreciates the support provided by the DIMPROD group. The author thanks the SNII for the designation, and more importantly, he truly appreciates the feedback on the ideas presented here provided by Professor Fidel Reyes Carmona.

References

1 J. Luo, *J. Am. Ceram. Soc.*, 2012, **95**(8), 2358–2371.
2 X. J. Liu, K. Oikawa, I. Ohnuma, R. Kainuma and K. Ishida, *JOM*, 2003, **55**(12), 53–59.
3 V. Raghavan, *J. Phase Equilibria Diffus.*, 2015, **36**(2), 89–91.
4 G. Guisbiers, *Adv. Phys.: X*, 2019, **4**(1), 1668299.
5 M. A. Jabbareh and F. Monji, *Calphad*, 2018, **60**, 208–213.
6 Y. Magnin, A. Zappelli, H. Amara, F. Ducastelle and C. Bichara, *Phys. Rev. Lett.*, 2015, **115**(20), 205502.
7 J. Pohl, C. Stahl and K. Albe, *Beilstein J. Nanotechnol.*, 2012, **3**(1), 1–11.
8 M. Z. Chu, Y. Z. Qin, T. Xiao, W. Shen, T. Su, C. H. Hu, *et al.*, *Calphad*, 2021, **72**, 102233.
9 G. Abudukelimu, G. Guisbiers and M. Wautelet, *J. Mater. Res.*, 2006, **21**(11), 2829–2834.
10 K. Balasubramanian, S. Banik, S. Manna, S. Srinivasan and K. R. S. Subramanian Sankaranarayanan, *APL Mach. Learn.*, 2024, **2**(1), 16103.
11 S. Rana, D. S. Monder and A. Chatterjee, *Comput. Mater. Sci.*, 2024, **233**, 112727.
12 K. Tsutsui and K. Moriguchi, *Calphad*, 2021, **74**, 102303.
13 T. Abe, Y. Chen, A. Saengdeejimg and Y. Kobayashi, *Scr. Mater.*, 2018, **154**, 305–310.
14 W. Zhu, J. Zhang, J. Luo, C. Zeng, H. Su, J. Zhang, *et al.*, *Adv. Mater.*, 2023, **35**(2), 2208974.
15 C. Suryanarayana, *J. Mater. Sci.*, 2018, **53**(19), 13364–13379.
16 C. C. Koch, *Mater. Sci. Forum*, 1992, **88–90**, 243–262.
17 E. Nshimyimana, X. Su, H. Xie, W. Liu, R. Deng, T. Luo, *et al.*, *Sci. Bull.*, 2018, **63**(11), 717–725.
18 H. Rojas-Chávez, F. Reyes-Carmona and D. Jaramillo-Vigueras, *Mater. Res. Bull.*, 2011, **46**(10), 1560–1565.
19 H. Rojas-Chávez, F. Reyes-Carmona, L. Huerta and D. Jaramillo-Vigueras, *Mater. Res. Bull.*, 2013, **48**(4), 1381–1387.
20 H. Rojas-Chávez, F. Reyes-Carmona, L. Huerta and D. Jaramillo-Vigueras, *IOP Conf. Ser. Mater. Sci. Eng.*, 2013, **45**(1), 012028.
21 H. Rojas-Chávez, J. L. González-Domínguez, R. Román-Doval, J. M. Juárez-García, N. Daneu and R. Farías, *Mater. Sci. Semicond. Process.*, 2018, **86**, 128–138.
22 H. Rojas-Chávez, H. Cruz-Martínez, L. Huerta, F. Montejo-Alvaro, A. Ávila-García, M. A. Valdés-Madrigal, *et al.*, *Appl. Surf. Sci.*, 2021, **564**, 150455.
23 H. Rojas-Chávez, F. Reyes-Carmona, V. Garibay-Febles and D. Jaramillo-Vigueras, *J. Nanopart. Res.*, 2013, **15**(5), 1–11.
24 H. Rojas-Chávez, S. Díaz-de la Torre, D. Jaramillo-Vigueras and G. Plascencia, *J. Alloys Compd.*, 2009, **483**(1–2), 275–278.
25 H. Rojas-Chávez, A. Miralrio, H. Cruz-Martínez, G. Carbajal-Franco and M. A. Valdés-Madrigal, *Inorg. Chem.*, 2021, **60**(10), 7196–7206.
26 H. Rojas-Chávez, A. Miralrio, J. M. Juárez-García, G. Carbajal-Franco, H. Cruz-Martínez, F. Montejo-Alvaro, *et al.*, *Int. J. Mol. Sci.*, 2022, **23**(19), 11194.
27 H. Rojas-Chávez, A. Miralrio, J. M. Juárez-García, H. Cruz-Martínez, G. Carbajal-Franco and M. A. Valdés-Madrigal, *Appl. Surf. Sci.*, 2023, **639**, 158173.
28 H. Rojas-Chávez, J. M. Juárez-García, R. Herrera-Rivera, E. Flores-Rojas, J. L. González-Domínguez, A. Cruz-Orea, *et al.*, *J. Alloys Compd.*, 2020, **820**, 153167.
29 H. Rojas-Chávez, A. Miralrio, H. Cruz-Martínez, J. A. Martínez-Espinosa, G. Carbajal-Franco and J. M. Juárez-García, *Comput. Mater. Sci.*, 2022, **206**, 111291.
30 D. Risold, J. I. Nagata and R. O. Suzuki, *J. Phase Equilibria*, 1998, **19**(3), 213–233.
31 K. Gavrichev, A. Bolshakov, D. Kondakov, A. Khoroshilov and S. Denisov, *J. Therm. Anal. Calorim.*, 2008, **92**(3), 857–863.
32 P. Ruetschi, J. Sklarchuk and R. T. Angstadt, *Electrochim. Acta*, 1963, **8**(5), 333–342.
33 J. S. Anderson and M. Sterns, *J. Inorg. Nucl. Chem.*, 1959, **11**(4), 272–285.
34 A. Berthereau, Y. Le Luyer, R. Olazcuaga, G. Le Flem, M. Couzi, L. Canioni, *et al.*, *Mater. Res. Bull.*, 1994, **29**(9), 933–941.
35 M. A. K. Ahmed, H. Fjellvåg and A. Kjekshus, *Dalton Trans.*, 2000, **24**, 4542–4549.
36 L. Chen, T. Goto, R. Tu and T. Hirai, *International Conference on Thermoelectrics, ICT, Proceedings*, 1997, pp. 251–254, DOI: 10.1109/ICT.1997.667101.
37 L. V. Yashina, E. V. Tikhonov, V. S. Neudachina, T. S. Zyubina, A. N. Chaika, V. I. Shtanov, *et al.*, *Surf. Interface Anal.*, 2004, **36**(8), 993–996.

38 J. Galat, J. Haber, J. Nowotny and J. B. Wagner, *Oxid. Met.*, 1975, **9**(6), 497–506.
39 C. Artner and M. Weil, *J. Solid State Chem.*, 2013, **199**, 240–247.
40 S. L. James, C. J. Adams, C. Bolm, D. Braga, P. Collier, T. Frišcic, *et al.*, *Chem. Soc. Rev.*, 2011, **41**(1), 413–447.
41 H. Rojas-Chávez, H. Cruz-Martínez, E. Flores-Rojas, J. M. Juárez-García, J. L. González-Domínguez, N. Daneu, *et al.*, *Phys. Chem. Chem. Phys.*, 2018, **20**(42), 27082–27092.
42 K. Kunkel, E. Milke and M. Binnewies, *Eur. J. Inorg. Chem.*, 2015, **2015**(1), 124–133.
43 L. Chen, T. Goto, R. Tu and T. Hirai, *J. Jpn. Soc. Powder Powder Metall.*, 1997, **44**(7), 653–657.